Electrochimica Acta 65 (2012) 210–215

Contents lists available at SciVerse ScienceDirect

Electrochimica Acta

journal homepage: www.elsevier.com/locate/electacta

Support effects on the oxidation of ethanol at Pt nanoparticles

Reza B. Moghaddam, Peter G. Pickup*

Department of Chemistry, Memorial University of Newfoundland, St. John's, Newfoundland, Canada A1B 3X7

ARTICLE INFO

Article history:
Received 10 November 2011
Received in revised form 11 January 2012
Accepted 12 January 2012
Available online 20 January 2012

Keywords:
Ethanol
Oxidation
Oxide
Support
Platinum

ABSTRACT

The effects of metal oxide supports on ethanol oxidation have been investigated by drop coating Pt nanoparticles onto glassy carbon electrodes coated with thin layers of ruthenium oxide, tin oxide, a mixed Ru + Sn oxide, and onto an indium–tin oxide (ITO) electrode. All four oxide supports exhibited significant co-catalytic effects, with their effectiveness at low potentials increasing in the order Ru oxide < ITO < Ru + Sn oxide < Sn oxide. However, at higher potentials (e.g. 0.4 V vs. SCE) currents were higher for Pt supported on Ru oxide or Ru + Sn oxide than on Sn oxide, revealing mechanistic differences between the roles of Ru and Sn oxide. Although Sn oxide produced very high initial activities, ITO and Ru + Sn oxide provided more stable performances.

1. Introduction

The electrochemical oxidation of ethanol is currently attracting considerable interest due to its central importance in the development of direct ethanol fuel cells (DEFCs) [1–5]. A 2007 review of electrocatalysts for ethanol oxidation concluded that PtSn catalysts were the most active binary systems in acidic media, while addition of Ru resulted in the most promising ternary systems [3]. However, these systems promote the incomplete oxidation of ethanol to acetaldehyde and acetic acid in favour of its complete oxidation to carbon dioxide [3,6,7]. This leads to very low fuel efficiencies in DEFCs [2] and high levels of byproducts that would need to be destroyed or recycled.

The key challenge in developing catalysts for ethanol oxidation is to find systems that can efficiently break the C—C bond so that the complete oxidation to CO_2 can occur. To date, the highest yields of CO_2 have been obtained with pure Pt catalysts [7], which have low activities. Deposition of Pt on Sn oxide has been reported to increase its activity relative to codeposited PtSn [8], while a ternary $PtRhSnO_2$/C catalyst has been reported to split the C—C bond in ethanol at ambient temperature with close to 50% efficiency [9,10]. Density functional calculations indicated that interactions between the PtRh alloy and SnO_2 play a crucial role in C—C bond breaking [9]. A study of the effects of SnO_x islands on ethanol oxidation at a Pt(1 1 1) surface has suggested that the Sn oxide promotes the removal of CO at the Pt/SnO_x interfaces [11]. SnInO [12], SnO_2 treated with sulphuric acid [13], TiO_2 nano-rods [14], TiO_2 containing polyoxometallate modified Au nanoparticle [15], Ru containing pervosites [16] and $Sb_2O_5{\cdot}SnO_2$ [17] supports have also been shown to be effective for ethanol oxidation at Pt nanoparticles. These results suggest that the best approach to the development of high efficiency catalysts for ethanol oxidation may be through the use of oxide supports, since it is clear that the interactions between various oxides and Pt can significantly increase the current density for ethanol oxidation, and there is evidence that this can occur without greatly inhibiting its complete oxidation to carbon dioxide [9,10].

We have recently demonstrated that support effects in electrocatalysis can be unambiguously identified and quantitatively compared by applying monolayer quantities of preformed catalyst nanoparticles onto modified glassy carbon electrodes [18,19]. For example, it was shown that a thin layer of Ru oxide on the glassy carbon strongly promoted the oxidation of methanol at Pt, while a layer of polyaniline had mainly inhibitory effects [18]. This methodology has been applied here to investigate and compare the effects of various oxides on the oxidation of ethanol at supported Pt nanoparticles. Glassy carbon was used as a control support, while indium–tin oxide (ITO) and thin layers or Ru oxide, Sn oxide, and a mixed Ru—Sn oxide on glassy carbon are shown to provide activating support effects.

2. Experimental

2.1. Chemicals

Sulphuric acid (Fisher Scientific), anhydrous ethanol (Commercial Alcohols Inc.), $KRuO_4$ (Alfa Aesar), $SnCl_4{\cdot}5H_2O$ (Fisher Scientific), $H_2PtCl_6{\cdot}6H_2O$ (Alfa Aesar), potassium hydroxide (ACP

* Corresponding author. Tel.: +1 709 864 8657; fax: +1 709 864 3702.
E-mail address: ppickup@mun.ca (P.G. Pickup).

0013-4686/$ – see front matter © 2012 Elsevier Ltd. All rights reserved.
doi:10.1016/j.electacta.2012.01.042

Chemical Inc.), sodium citrate (Anachemia), sodium borohydride (Sigma–Aldrich), and Nafion™ solution (5%; Dupont) were used as received. All measurements were recorded at ambient temperature under a nitrogen atmosphere following purging for 15 min.

2.2. Preparation of Pt nanoparticles

$NaBH_4$(aq) (1.5 mL; 120 mM) was added dropwise to a stirred solution of 10 mL of 3 mM H_2PtCl_6(aq) mixed with 0.6 mL of 50 mM aqueous sodium citrate [20]. Following stirring for a further 2 h, the resulting grey colloidal Pt nanoparticle solution was stored in a fridge. This stock solution was diluted by a factor of 20 prior to use with water and Nafion solution to give 1.2 μg mL^{-1} Nafion. X-ray diffraction measurements indicated that the average particle diameter was 5.0 ± 0.4 nm.

2.3. Working electrode preparation

Glassy carbon electrodes (GC; CH Instruments; 0.071 cm^2) were polished with 0.05 μm alumina and rinsed well with water before use. Electrodes were coated with a thin film (ca. 25 nm) of hydrous Ru oxide (GC/Ru oxide) as previously described [18]. Spontaneous deposition was also used to prepare GC/Sn oxide electrodes, by immersion of preconditioned (E = −0.5 V, t = 300 s in 0.1 M H_2SO_4) GC electrodes in a neutral aqueous $SnCl_4$ solution (0.05 M) for 15 min. Spontaneous codeposition was used to prepare GC/Ru_xSn_{x-1} oxide electrodes, whereby a preconditioned (E = −0.5 V, t = 300 s in 0.1 M H_2SO_4) GC electrode was placed in 0.05 M $KRuO_4$ + 0.05 M $SnCl_4$ (in 0.1 M KOH) for 15 min. The GC, ITO (on glass; Donnelly Corp.), GC/Sn oxide and GC/Ru_xSn_{1-x} oxide/Pt electrodes were then drop coated with 12.5 μL of the diluted Nafion containing Pt colloid to obtain GC/Pt, ITO/Pt, GC/Ru oxide/Pt, GC/Sn oxide/Pt and GC/Ru_xSn_{1-x} oxide/Pt electrodes with Pt loadings of 3.0×10^{-7} g (4.3 μg cm^{-2}) with 5% Nafion by mass relative to Pt.

Analysis of two of these electrodes by ICP-MS gave the following results:

GC/Sn oxide/Pt: Sn = 0.33–0.34 μg, Pt = 0.39 μg
GC/Ru_xSn_{x-1} oxide/Pt: Ru = 1.5 μg, Sn = 0.32 μg, Pt = 0.41 μg

The Ru_xSn_{x-1} oxide composition was therefore $Ru_{0.85}Sn_{0.15}$ oxide, and the Pt loadings were close to the targeted value. Based on the densities of SnO_2 and RuO_2 (6.95 g cm^{-3} and 6.97 g cm^{-3}, respectively), the thicknesses of the Sn oxide and $Ru_{0.85}Sn_{0.15}$ oxide films can be estimated to have been ca. 9 nm and 40 nm, respectively.

2.4. Instrumentation

An EG&G Model 273A Potentiostat/Galvanostat run by a PC through M270 commercial software was used for voltammetric measurements. A saturated calomel electrode (SCE) and a platinum wire formed the reference and counter electrodes, respectively.

A Model FEI Quanta 400 environmental SEM was used to perform scanning electron microscopy (SEM) measurements. For transmission electron microscopy (TEM), the colloidal Pt nanoparticle solution was diluted with ethanol and sonicated for some minutes. A drop of the mixture was then placed on a 200 mesh copper grid with a carbon support film. The grid was allowed to dry overnight and then observed under a Model JEOL 2011 transmission electron microscope (The Microscopy and Microanalysis Facility, University of New Brunswick). AFM measurements were conducted with a Quesant Q-Scope 350 using a smooth glassy carbon plate (SPI Supplies, USA) as the substrate.

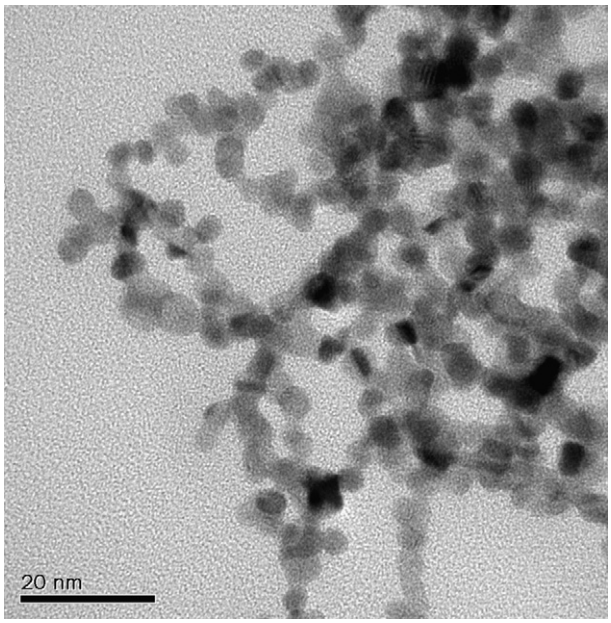

Fig. 1. TEM of the Pt nanoparticles.

3. Results and discussion

3.1. Characterization of the nanoparticles and electrodes

Fig. 1 shows a TEM image of the Pt nanoparticles. There is a relatively narrow size distribution with an average diameter of 5.0 ± 1.3 nm that is consistent with the XRD measurement. Based on the surface area to mass ratio calculated for particles of this size, the loading of 3.0×10^{-7} g Pt applied to each electrode would correspond to a real geometric Pt surface area of 0.17 cm^2.

Fig. 2 shows SEM and AFM images of a GC plate coated with 3.0×10^{-7} g of Pt nanoparticles with 5% Nafion by mass following washing with deionized water to remove residual salts from the synthesis solution. It can be seen from the SEM image that the Pt + Nafion mixture formed an uneven coating, as a result of which some regions consisted of aggregates and some regions were bare. AFM confirmed the uneven Pt + Nafion distribution, displaying aggregates as high as 70 nm. The average layer thickness of 14 nm seen in Fig. 2B is reasonably consistent with the quantity of Pt applied to the electrode, which was roughly equivalent to one close-packed monolayer of 5 nm particles, and the volume ratio of Pt to Nafion of ca. 1:1.

Fig. 3 shows overlaid cyclic voltammograms of GC/Pt, ITO/Pt, GC/Ru oxide/Pt, GC/Sn oxide/Pt and GC/$Ru_{0.85}Sn_{0.15}$ oxide/Pt electrodes in 0.1 M H_2SO_4. The forward scan (anodic) for the GC/Pt electrodes shows peaks centered at −0.13 and −0.08 V assigned to hydrogen desorption, followed by the onset of Pt oxide (PtO) formation from ∼0.4 V. A well-defined peak for PtO reduction can be seen at ca. 0.47 V, following which hydrogen adsorption and hydrogen evolution occur beyond −0.04 V to terminate the cathodic scan. These features are generally similar for the other electrodes. Nevertheless, the GC/Ru oxide/Pt, GC/Sn oxide/Pt, and particularly the GC/$Ru_{0.85}Sn_{0.15}$ oxide/Pt show larger background currents, and the signals assigned to hydrogen desorption/adsorption were suppressed in some cases. In contrast, ITO/Pt had a low background current and its voltammogram was most similar to that of GC/Pt.

Electrochemically active areas estimated from the H adsorption waves in Fig. 3 were 0.078, 0.071, 0.055, 0.043, and 0.078 cm^2, respectively, for the GC/Pt, ITO/Pt, GC/Ru oxide/Pt, GC/Sn oxide/Pt and GC/$Ru_{0.85}Sn_{0.15}$ oxide/Pt electrodes. These values correspond to electrochemical utilizations (active area/geometric area)

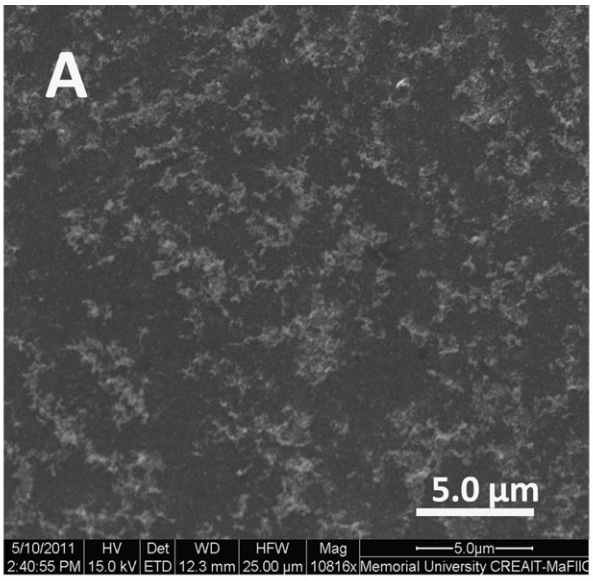

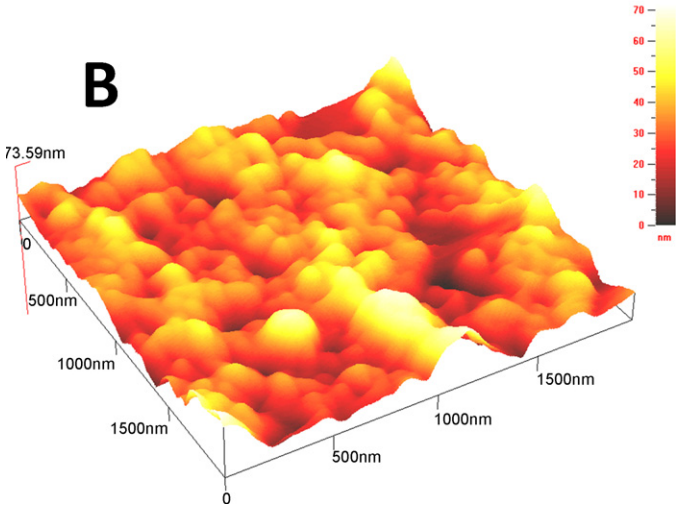

Fig. 2. SEM (A) and AFM (B; $2 \times 2\,\mu m \times 74\,nm$) images of ca. $4.3\,\mu g\,cm^{-2}$ of Pt nanoparticles + Nafion on GC.

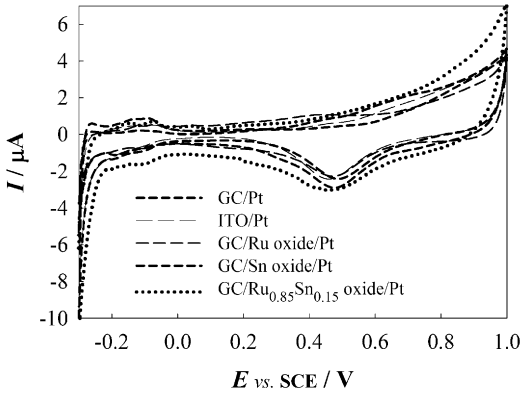

Fig. 3. Cyclic voltammograms ($10\,mV\,s^{-1}$) in 0.1 M H_2SO_4 of GC, ITO, GC/Ru oxide, GC/Sn oxide and GC/$Ru_{0.85}Sn_{0.15}$ oxide electrodes coated with $4.3\,\mu g\,cm^{-2}$ of Pt nanoparticles.

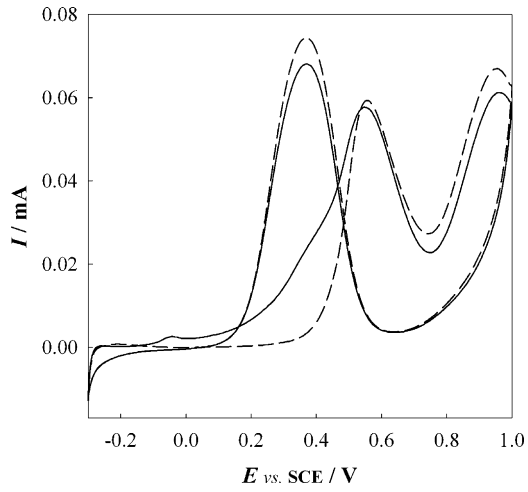

Fig. 4. Cyclic voltammogram ($10\,mV\,s^{-1}$; 1st scan solid, 2nd scan dashed) in 0.1 M H_2SO_4 containing 0.2 M ethanol of a GC electrode coated with $4.3\,\mu g\,cm^{-2}$ of Pt nanoparticles.

ranging from 26% to 46%. Previously, it has been shown that use of the hydrogen adsorption waves for the type of GC/Pt electrode used here underestimates the electrochemically active Pt area relative to use of the oxide stripping peak or Cu underpotential deposition [18]. It is therefore not clear that the differences in apparent utilizations between electrodes observed here (in Fig. 3) are meaningful, or even significant relative to the experimental uncertainty.

3.2. Ethanol oxidation

For each electrode, cyclic voltammetry in the presence of ethanol was conducted immediately following the cyclic voltammetry in 0.1 M H_2SO_4 shown in Fig. 3. The electrode, initially at −0.3 V, was raised out of the electrolyte solution while ethanol was added and then immersed into the mixed 0.1 M H_2SO_4 + 0.2 M ethanol solution. A nitrogen atmosphere was maintained during this procedure which typically took ca. 30 s.

Fig. 4 shows the first two CV scans for a GC/Pt electrode in the presence of ethanol. The onset of ethanol oxidation during the forward scan of the first cycle is very early, at ca. 0 V. A small peak appears at ca. −0.05 V, followed by a rising current to a dominant oxidation peak centered at 0.56 V. There is a weakly defined shoulder at about 0.38 V and a second peak at +0.95 V. The reverse scan of the first cycle consists of a large anodic peak at 0.37 V that can be attributed to rapid oxidation of ethanol at the clean Pt produced by reduction of the Pt oxide layer formed at higher potentials. On the second cycle, the onset of ethanol oxidation is shifted to a much higher potential (ca. 0.3 V) and the shoulder at ca. 0.38 V is absent. This is discussed in Section 3.3.

Fig. 5 compares the first forward scans for ethanol oxidation at GC/Pt, ITO/Pt, GC/Ru oxide/Pt, GC/Sn oxide/Pt and GC/$Ru_{0.85}Sn_{0.15}$ oxide/Pt electrodes. The reverse scans were not notably influenced by the presence of the oxide layers, and so are not presented. At potentials below ~0.4 V, the GC/Sn oxide/Pt and GC/$Ru_{0.85}Sn_{0.15}$ oxide/Pt electrodes gave markedly higher currents than the others, with both showing a large oxidation peak at ca. 0.3 V. The response of the GC/Ru oxide/Pt electrode in this region was somewhat better than that at the GC/Pt electrode, while ITO/Pt was somewhat better than GC/Ru oxide/Pt. These results clearly indicate that Sn oxide facilitates the decomposition of ethanol and/or has a synergetic/co-catalytic effect on Pt in the oxidation of ethanol. The presence of Ru in the mixed $Ru_{0.85}Sn_{0.15}$ oxide does not significantly change the effect of the Sn, while the presence of In in the ITO appears to diminish its effect.

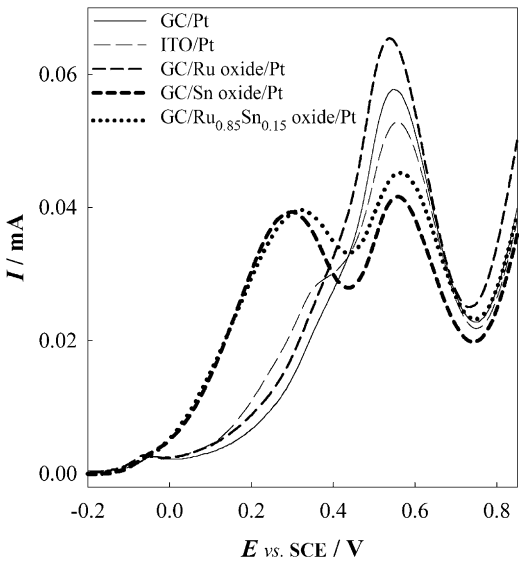

Fig. 5. First anodic scans of cyclic voltammograms (10 mV s^{-1}) for GC/Pt, ITO/Pt, GC/Ru oxide/Pt, GC/Sn oxide/Pt and GC/$Ru_{0.85}Sn_{0.15}$ oxide/Pt electrodes in 0.1 M H_2SO_4 containing 0.2 M ethanol.

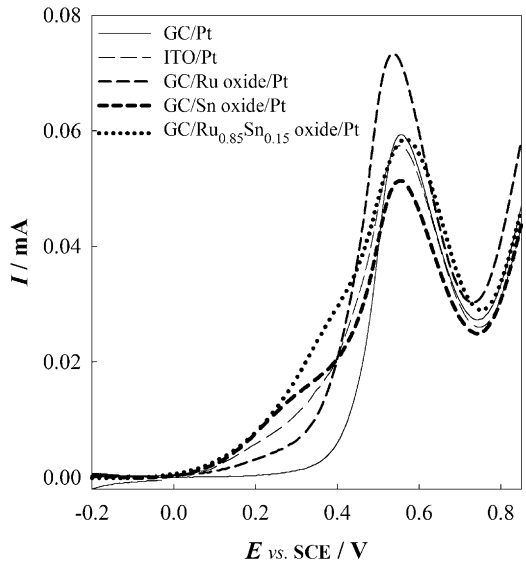

Fig. 6. Second anodic scans of cyclic voltammograms (10 mV s^{-1}) for GC/Pt, ITO/Pt, GC/Ru oxide/Pt, GC/Sn oxide/Pt and GC/$Ru_{0.85}Sn_{0.15}$ oxide/Pt electrodes in 0.1 M H_2SO_4 containing 0.2 M ethanol.

The striking contrast between the effects of Ru oxide and Sn oxide seen in Fig. 5 has important mechanistic implications. Since Ru oxide is known to be very effective at shifting the onset of CO oxidation to lower potentials, its relatively small influence here implies that poisoning of the Pt by CO was not severe at potentials below 0.4 V. Thus the role of Sn may not be related to its ability to inhibit CO formation or promote CO oxidation.

Inspection of the linear sweep voltammograms in Fig. 5 over the 0.4–0.8 V range reveals additional insight into the roles of the metal oxides. In all cases, the peak at ca. 0.55 V can be primarily attributed to the oxidation of ethanol to CO_2 through an adsorbed CO intermediate on the Pt nanoparticles. The height of this peak shows a rough inverse correlation with the onset of ethanol oxidation, with GC/Pt and GC/Ru oxide/Pt showing the highest currents in the region, while GC/Sn oxide/Pt and GC/$Ru_{0.85}Sn_{0.15}$ oxide/Pt gave the lowest. This may suggest that the presence of Sn promotes the direct oxidation of ethanol to acetaldehyde and acetic acid over the formation of CO_2 via an adsorbed CO intermediate.

Although the results shown in Fig. 5 provide some important insights into the mechanistic role of the Sn oxide supports, they are not very relevant to their use in fuel cells where high steady state ethanol oxidation rates are required. In all cases, currents at potentials below ca. 0.4 V were diminished considerably on the second cycle, as illustrated for CG/Pt in Fig. 4. For GC/Pt, ITO/Pt, GC/Ru oxide/Pt and GC/$Ru_{0.85}Sn_{0.15}$ oxide/Pt electrodes, the changes after the 2nd cycle were relatively small (not shown). However, for GC/Sn oxide/Pt electrodes the currents below ca. 0.4 V continued to decrease significantly over many cycles. Nonetheless, the superior performances of the ITO/Pt, GC/Sn oxide/Pt and GC/$Ru_{0.85}Sn_{0.15}$ oxide/Pt electrodes over GC/Pt and GC/Ru oxide/Pt were maintained over multi cycles. This is illustrated in Fig. 6 which shows the 2nd cycles of the voltammograms for all of the electrodes.

These changes in the cyclic voltammograms with cycling make it very difficult to accurately assess the effects of the various oxide supports on ethanol oxidation at the Pt nanoparticles. More definitive comparisons were therefore obtained by chronoamperometry. A voltammogram of each electrode was obtained in 0.1 M H_2SO_4 prior to these experiments but, in order to preserve their initial activity, no voltammetry was performed in the presence of ethanol. Sequential chronoamperometry experiments were then run at 0 V, 0.1 V, 0.2 V, 0.3 V, and 0.4 V, but only the 0.1 V and 0.4 V results are shown here.

Chronoamperometric oxidation of ethanol at 0.1 V at GC/Pt, ITO/Pt, GC/Ru oxide/Pt, GC/Sn oxide/Pt and GC/$Ru_{0.85}Sn_{0.15}$ oxide/Pt electrodes is presented in Fig. 7. Consistent with the CVs, GC/Pt and GC/Ru oxide/Pt were much less active at 0.1 V than the ITO/Pt, GC/Sn oxide/Pt and GC/$Ru_{0.85}Sn_{0.15}$ oxide/Pt electrodes. The GC/Pt electrode initially gave a higher current than the GC/Ru oxide/Pt electrode but its current decayed more rapidly. The superior longer term activity of the GC/Ru oxide/Pt electrode is consistent with the ability of Ru oxide to facilitate the oxidation of CO, which is known to poison Pt during ethanol oxidation.

The presence of Sn oxide in the support for the Pt nanoparticles greatly enhanced their activity for ethanol oxidation at 0.1 V, with the greatest effect seen for the GC/Sn oxide/Pt electrode in Fig. 7. The activity of the GC/$Ru_{0.85}Sn_{0.15}$ oxide/Pt electrode was only slightly lower, while the activity of the ITO/Pt electrode was significantly lower. Current decay rates were similar for the GC/Ru oxide/Pt, GC/Sn oxide/Pt and GC/$Ru_{0.85}Sn_{0.15}$ oxide/Pt electrodes, but slightly higher for the ITO/Pt electrode. Fig. 8 presents chronoamperometric profiles at a more positive potential of 0.4 V. Here, the GC/Pt electrode gave the lowest current at all times. For times less than ca. 150 s, the electrodes with oxide supports

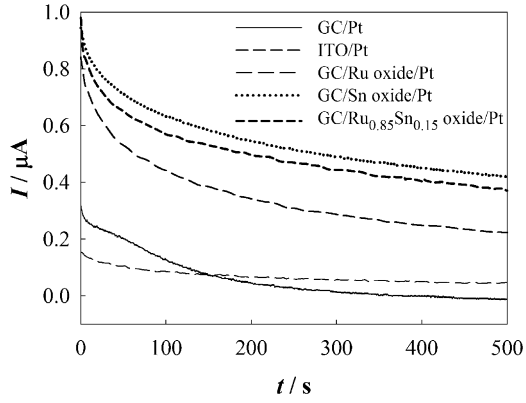

Fig. 7. Chronoamperometry at +0.1 V for GC/Pt, ITO/Pt, GC/Ru oxide/Pt, GC/Sn oxide/Pt and GC/$Ru_{0.85}Sn_{0.15}$ oxide/Pt electrodes in 0.1 M H_2SO_4 containing 0.2 M ethanol.

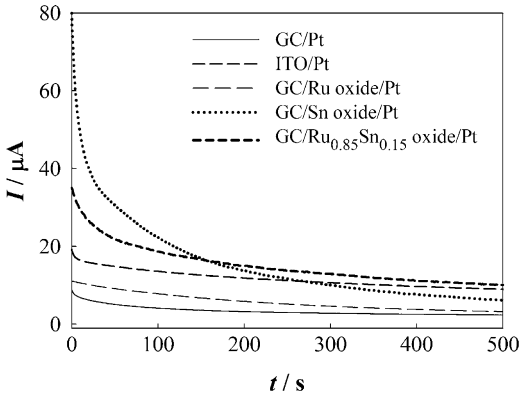

Fig. 8. Chronoamperometry at +0.4 V for GC/Pt, ITO/Pt, GC/Ru oxide/Pt, GC/Sn oxide/Pt and GC/$Ru_{0.85}Sn_{0.15}$ oxide/Pt electrodes in 0.1 M H_2SO_4 containing 0.2 M ethanol.

followed the same activity trend as they did at 0.1 V. At short times the activity of the GC/Sn oxide/Pt electrode was much higher than for the others, but it decayed much more rapidly. The GC/$Ru_{0.85}Sn_{0.15}$ oxide/Pt electrode also had a relatively high initial activity and its decay rate was lower than for GC/Sn oxide/Pt. Consequently, it gave the best longer term (>150 s) activity. ITO/Pt gave a lower initial current but exhibited the lowest decay rate, while GC/Ru oxide/Pt was inferior both in terms of initial current and decay rate.

3.3. Mechanistic insights

The electrocatalytic oxidation of ethanol at Pt begins with its oxidative adsorption (reactions (1) and (2)) followed by its oxidative dissociation to a mixture of $-CH_x$ and oxygen containing species (reactions (3) and (4)) [21–23].

$$CH_3CH_2OH + Pt \rightarrow Pt{-}O{-}CH_2CH_3 + H^+ + e^- \quad (1)$$

$$CH_3CH_2OH + Pt \rightarrow Pt{-}CH(OH)CH_3 + H^+ + e^- \quad (2)$$

$$Pt{-}O{-}CH_2CH_3 \text{ or } Pt{-}CH(OH)CH_3 \rightarrow Pt{-}CHOCH_3 + H^+ + e^- \quad (3)$$

$$Pt{-}O{-}CH_2CH_3 \text{ or } Pt{-}CH(OH)CH_3 \rightarrow Pt{-}CH_x + Pt{-}CH_yO + (5{-}x{-}y)H^+ + (5{-}x{-}y)e^- \quad (4)$$

Both the adsorbed Pt—CH_x and Pt—CH_yO type species can be further oxidized to adsorbed CO (e.g. reaction (5)) and then to CO_2 (reaction (6)).

$$Pt{-}CH_2O \rightarrow Pt{-}CO + 2H^+ + 2e^- \quad (5)$$

$$Pt{-}CO + Pt{-}OH \rightarrow 2Pt + CO_2 + H^+ + e^- \quad (6)$$

The oxidative adsorption of ethanol at Pt is generally followed by *in situ* vibrational spectroscopy [23], usually by monitoring the adsorbed CO produced by reactions such as (5). Complementary information can be obtained by measuring the CO_2 produced by oxidative stripping of adsorbates by differential electrochemical mass spectrometry (DEMS) [24,25], and from quantum chemistry calculations [22]. The oxidative adsorption of ethanol on Pt can be completely suppressed by underpotentially deposited hydrogen at low potentials (e.g. 0.06 V vs. RHE [24]), but produces substantial coverages of CO and other adsorbates at higher potentials [21,23,24]. Oxidation of these adsorbates to CO_2 begins at ca. 0.5 V vs. RHE [24] (~0.25 V vs. SCE), which coincides approximately with a decrease in the intensity of the vibrational response due to adsorbed CO [21,23]. However, the amount of CO_2 produced corresponds to ≤60% of a CO monolayer, indicating the presence of other adsorbates that cannot readily be oxidized. For the adsorbed species that are oxidized to CO_2, 2.2–5.9 electrons are involved per CO_2 molecule, depending on the adsorption and stripping potentials [24]. This indicates that various oxidizable Pt—CH_x and Pt—CH_yO species are formed during the oxidative adsorption of ethanol on Pt.

In light of the above discussion, the large differences between the first and subsequent anodic voltammetric scans for ethanol oxidation seen in this work (e.g. Fig. 4) can be explained by the changing populations of the various adsorbates that are formed. Before the first scan, it is clear that a diverse range of one and two carbon adsorbates would be present. The dominate species would be Pt—CO, which is oxidized to CO_2 during the main peak seen at ca. +0.55 V for scans at all electrodes. The small peak seen at ca. −0.05 V on the first scan for all electrodes may be due to adsorbed H, while the broad shoulders are presumably due to the oxidation of species such as Pt—O—CH_2CH_3, Pt—$CH(OH)CH_3$, Pt—CH_3 and Pt—CH_2O. The absence of these features on the second anodic scan at the GC/Pt electrode (Fig. 4) suggests that CO is the predominant adsorbate formed during the cathodic scan. The fact that the broad shoulder prior to the +0.55 V peak persists to varying extents for the ITO/Pt, GC/Ru oxide/Pt, GC/Sn oxide/Pt and GC/$Ru_{0.85}Sn_{0.15}$ oxide/Pt electrodes (Fig. 6) indicates that the oxide supports facilitate the oxidation of adsorbed CO and/or may play other roles in promoting ethanol oxidation.

The role of the Ru oxide support is reasonably clear because it is consistent with the well known bifunctional mechanism for CO oxidation at Pt—Ru electrodes, as shown in reaction (7).

$$Pt{-}CO + Ru{-}OH \rightarrow Pt + Ru + CO_2 + H^+ + e^- \quad (7)$$

Since Ru—OH forms at lower potentials than Pt—OH, reaction (7) occurs at lower potentials than reaction (6). It has been previously demonstrated that this occurs for methanol oxidation at GC/Ru oxide/Pt electrodes, where the predominant adsorbate is CO [18]. The shift in the oxidation wave in Fig. 6 for GC/Ru oxide/Pt relative to GC/Pt is similar to that seen for methanol oxidation, suggesting a similar mechanistic role for the Ru oxide support.

In the following discussion of the literature on the activities and mechanisms of PtRu and PtSn catalysts and the roles of the various oxide supports employed here, we use the term PtM (where M is Ru or Sn) to refer to results for either PtM alloys or various types of mixed Pt + M oxide catalysts. Although this may result in some inaccuracies in the comparisons [26], it reflects the observation that these two types of catalyst system generally behave very similarly, and appear to operate by similar mechanisms. This is due to the fact that Ru and Sn at the surfaces of alloy catalysts are usually present in the form of oxides [26].

Although PtRu systems can promote ethanol oxidation by the bifunctional mechanism shown in reaction (7), it is well known that PtSn systems are more effective promoters. In contrast, PtRu systems are much more effective for methanol oxidation than PtSn systems [27,28]. These differences can possibly be explained by the observation that Sn species (oxides) promote CO oxidation by electronic effects (ligand effects) that weaken the Pt—CO bond, rather than the bifunctional mechanism [26].

For ethanol oxidation, it has been reported that PtSn is more effective than PtRu at low potentials while PtRu becomes more effective at higher potentials [27,29]. The results shown in Figs. 6, 7 and 8 are consistent with this, with the GC/Ru oxide/Pt electrode showing the largest currents at potentials above ca. 0.4 V (Fig. 6), but all of the Sn oxide containing electrodes being more effective at 0.4 V and lower. Although we cannot yet provide a full explanation of these results, it does appear that the electronic effect of Sn oxide containing supports contribute to the removal of CO_{ads} at lower potentials than the bifunctional effect of the Ru oxide support. In terms of initial activity at low potentials, the pure Sn oxide support was better than either of the mixed oxides, which

can reasonably be attributed to the higher Sn concentration at the Pt surface. However, the presence of either In or Ru in the oxide significantly stabilizes the performance at potentials above ca. 0.1 V (see Fig. 8), and makes ITO and Ru_xSn_{x-1} oxide supports attractive for further investigation.

Finally, it is necessary to consider how the oxide supports employed here are able to induce similar bifunctional and electronic effects to those previously documented for PtM alloys and mixed Pt + M oxide catalysts. The bifunctional effects are addressed by work on systems in which the distance between catalyst pairs has been experimentally controlled. For example, Abruna et al. were able to demonstrate "electrocatalytic synergy" in the oxidation of CO between an Ru scanning tunnelling microscopy tip and a Pt substrate, via the bifunctional mechanism shown in Eq. (7) [32]. CO adsorbed on the Pt was oxidized at lower overpotentials when the Ru tip was brought close to its surface, with density functional theory calculations indicating that a critical distance of less than ca. 0.4 nm would be required for reaction (7) to occur. Sustained CO oxidation currents were observed due to surface diffusion of CO to the Ru tip. It is clear from these results that bifunctional oxidation of adsorbed CO on Pt nanoparticles will occur in a sustained fashion whenever there is contact (or even very close proximity) between any regions of the particles and a suitable metal oxide, regardless of whether the oxide is deposited onto the particles [11] or whether the particles are deposited on a metal oxide support. In addition, it is possible for particles of two different metals (or an oxide and a metal), such as Pt and Ru, in close proximity to exhibit synergistic effects due to chemical transfer of metal atoms via dissolution and redeposition [33].

Electronic effects between oxide supports and Pt nanoparticles have been extensively investigated [34 and references therein]. For example, in the case on Pt on TiO_2 [34] partial charge transfer from the substrate to Pt has been observed by X-ray photoelectron spectroscopy, which was correlated to increased activity to oxygen reduction.

4. Conclusions

The results presented here show unambiguously that both Ru and Sn containing oxide supports promote the oxidation of ethanol at Pt nanoparticles relative to a glassy carbon support. The methodology employed allows clear comparisons to be made between supports and will aid in the understanding of real catalysts which contain complex mixtures of alloyed and oxidized components [3,30,31] and for which compositions and structures are less certain. The use of preformed pure Pt nanoparticles ensures that the support does not influence their composition, particle size and distribution, or shape, while the use of thin support layers and Pt nanoparticle layers negates transport effects. The observed differences between the effects of Sn oxide and Ru oxide can therefore be attributed to differences in catalytic mechanisms, which appear to be dominated by a bifunctional mechanism for Ru oxide and electronic (ligand) effects for Sn oxide and mixed oxides containing Sn.

Acknowledgements

This work was supported by the Natural Sciences and Engineering Research Council of Canada and Memorial University. We also thank Dr. Louise Weaver at The Microscopy and Microanalysis Facility, University of New Brunswick, for making the TEM measurements.

References

[1] C. Lamy, A. Lima, V. LeRhun, F. Delime, C. Coutanceau, J.M. Leger, J. Power Sources 105 (2002) 283.
[2] F. Vigier, S. Rousseau, C. Coutanceau, J.M. Leger, C. Lamy, Top. Catal. 40 (2006) 111.
[3] E. Antolini, J. Power Sources 170 (2007) 1.
[4] S.Q. Song, V. Maragou, P. Tsiakaras, J. Fuel Cell Sci. Technol. 4 (2007) 203.
[5] U.B. Demirci, J. Power Sources 169 (2007) 239.
[6] S. Rousseau, C. Coutanceau, C. Lamy, J.M. Leger, J. Power Sources 158 (2006) 18.
[7] A. Ghumman, G. Li, D.V. Bennett, P.G. Pickup, J. Power Sources 194 (2009) 286.
[8] L.H. Jiang, G.Q. Sun, S.G. Sun, J.G. Liu, S.H. Tang, H.Q. Li, B. Zhou, Q. Xin, Electrochim. Acta 50 (2005) 5384.
[9] A. Kowal, M. Li, M. Shao, K. Sasaki, M.B. Vukmirovic, J. Zhang, N.S. Marinkovic, P. Liu, A.I. Frenkel, R.R. Adzic, Nat. Mater. 8 (2009) 325.
[10] M. Li, A. Kowal, K. Sasaki, N. Marinkovic, D. Su, E. Korach, P. Liu, R.R. Adzic, Electrochim. Acta 55 (2010) 4331.
[11] W.P. Zhou, S. Axnanda, M.G. White, R.R. Adzic, J. Hrbek, J. Phys. Chem. C 115 (2011) 16467.
[12] J. Mann, N. Yao, A.B. Bocarsly, Langmuir 22 (2006) 10432.
[13] X.W. Zhang, H. Zhu, Z.J. Guo, Y.S. Wei, F.H. Wang, J. Power Sources 196 (2011) 3048.
[14] X.S. He, C.G. Hu, J. Power Sources 196 (2011) 3119.
[15] S. Zoladek, I.A. Rutkowska, P.J. Kulesza, Appl. Surf. Sci. 257 (2011) 8205.
[16] A.D. Lan, A.S. Mukasyan, Ind. Eng. Chem. Res. 47 (2008) 8989.
[17] A.O. Neto, M. Brandalise, R.R. Dias, J.M.S. Ayoub, A.C. Silva, J.C. Penteado, M. Linardi, E.V. Spinace, Int. J. Hydrogen Energy 35 (2010) 9177.
[18] R.B. Moghaddam, P.G. Pickup, Electrochem. Commun. 13 (2011) 704.
[19] R.B. Moghaddam, P.G. Pickup, Electrocatalysis 2 (2011) 159.
[20] J. Yang, J.Y. Lee, H.-P. Too, Anal. Chim. Acta 571 (2006) 206.
[21] F. Vigier, C. Coutanceau, A. Perrard, E.M. Belgsir, C. Lamy, J. Appl. Electrochem. 34 (2004) 439.
[22] H.F. Wang, Z.P. Liu, J. Am. Chem. Soc. 130 (2008) 10996.
[23] R.B. Kutz, B. Braunschweig, P. Mukherjee, R.L. Behrens, D.D. Dlott, A. Wieckowski, J. Catal. 278 (2011) 181.
[24] H. Wang, Z. Jusys, R.J. Behm, Fuel Cells 4 (2004) 113.
[25] H.S. Wang, H.D. Abruna, in: A. Bocarsly, D.M.P. Mingos (Eds.), Structure and Bonding: Fuel Cells and Hydrogen Storage, vol. 141, Springer-Verlag, Berlin, 2011, p. 33.
[26] F.J. Scott, S. Mukerjee, D.E. Ramaker, J. Phys. Chem. C 114 (2010) 442.
[27] W.J. Zhou, B. Zhou, W.Z. Li, Z.H. Zhou, S.Q. Song, G.Q. Sun, Q. Xin, S. Douvartzides, A. Goula, P. Tsiakaras, J. Power Sources 126 (2004) 16.
[28] G. Li, P.G. Pickup, J. Power Sources 173 (2007) 121.
[29] H.Q. Li, G.Q. Sun, L. Cao, L.H. Jiang, Q. Xin, Electrochim. Acta 52 (2007) 6622.
[30] E. Antolini, E.R. Gonzalez, Catal. Today 160 (2011) 28.
[31] C.W. Liu, Y.W. Chang, Y.C. Wei, K.W. Wang, Electrochim. Acta 56 (2011) 2574.
[32] L. Zhuang, J. Jin, H.D. Abruna, J. Am. Chem. Soc. 129 (2007) 11033.
[33] B. Wickman, Y.E. Seidel, Z. Jusys, B. Kasemo, R.J. Behm, ACS Nano 5 (2011) 2547.
[34] A. Lewera, L. Timperman, A. Roguska, N. Alonso-Vante, J. Phys. Chem. C 115 (2011) 20153.